Polarization of THz Signals Using Graphene-Based Metamaterial Structure

Vishal Sorathiya and Sunil Lavadiya

Abstract Graphene-based Terahertz devices have attracted huge attention because of their ultrathin design and tunable property. The graphene-based polarizer can be formed using a single or multilayer of graphene sheet over the dielectric substrate. The different shapes and size of the engraved graphene geometry make possible to design different band and different mode of the polarizer which was ultrathin in design. The graphene-assisted polarizer also has the tunable by various physical parameters such as chemical potential, frequency, scattering rate. The graphene-based polarizer also provided unusual material properties like negative refractive index which makes the overall polarizer structure a metamaterial device. The proposed book chapter provides the fundamentals of graphene-based polarization devices. The chapter includes the mathematical modeling of the graphene-based polarizers devices and numerical investigation techniques used to identify the performance of the graphene-based polarizer structure. The chapter also includes a detailed comparative analysis of the previously published and available polarization devices in the market.

Keywords Graphene · Polarizer · Terahertz · Tunability

1 Introduction

Metamaterials (MMs), a modern form of the artificial substance that was recently investigated in terms of their non-traditional electromagnetic properties. These features are used to achieve numerous results such as negative refractive index [1], perfect lensing [2], bolometer [3], etc. On the other way, Graphene owns exceptional optical, electrical, and mechanical properties, such as large young modules, high

V. Sorathiya (✉) · S. Lavadiya
Department of Information and Communication Technology, Marwadi University, Rajkot, Gujarat 360002, India
e-mail: vishal.sorathiya@marwadieducation.edu.in

S. Lavadiya
e-mail: sunil.lavadiya@marwadieducation.edu.in

thermal conductivity, and massive carrier mobility [4]. Graphene material can be realized with the bandgap structure of Dirac tapered. Graphene also offers the properties of linear dispersion. Graphene is a one-atom-thick two-dimensional material that provides electrical and optical tunability over the ultra-wide range of THz and GHz [5] frequency. It is also attracted huge attention for research on preparation methods of graphene and its composition material. Similarly, the research community also identifying the various material property extraction from graphene and its composite devices. The property of the single-layer graphene can be controlled by temperature, scattering rate, chemical potential, and frequency [6]. Several devices were studied previously for Gigahertz to Terahertz region for achieving wide-angle [7], perfect absorption, tunability [8], and polarization-insensitive [9]. These types of properties of graphene provide the scope to design different tunable graphene-based photonics components like absorber [10], THz antenna[11], polarizer [12], grating structure [13, 14], Frequency selective surfaces [8], and bandpass filters. The current metamaterial does not have features of tunability. The conventional metamaterial is realized by the different layers of metal, Si_3N_4, SiO_2, and Al material. It is possible to achieve the tunable feature only with the thicker size of conventional material. The limitation of the size (specially thickens) and tunability can be fulfilled by the graphene-assisted metamaterial structures. Al, silica and Au substrate are used to form the single-layered graphene-based metamaterial devices. There are different shapes like *T* shaped [15], *L* shaped [16], rectangular split ring-shaped, *C* shaped [12] are engraved on graphene sheets to realize metamaterial polarizer. The graphene-based polarizer with composited graphene metallic wire grid array is one of the famous types of the polarizer to fabricate. There is wide use of the graphene-based polarizer in various applications like an attenuator, modulator, photonics sensor, etc.

2 Graphene Conductivity Model

The single layer of the graphene sheet between two different materials has been depicting as shown in Fig. 1. The sheet of graphene is considered as laterally infinite over the *x-z* plane. Graphene is interfaced as $\mu_1\varepsilon_1$ for $y > 0$ and $\mu_2\varepsilon_2$ for $y \leq 0$ between two mediums as shown in Fig. 1. Here we may consider the all-parameters values consisting of complex terms. The proposed graphene structure can be considered as ultrathin with a two-sided surface conductivity model with surface conductivity $\sigma(\omega, \mu_c, \Gamma, T)$. The conductivity of the graphene is considered by Kubo's Formula [6, 17, 18]. The equation of the surface conductivity model is shown in Eq. 1.
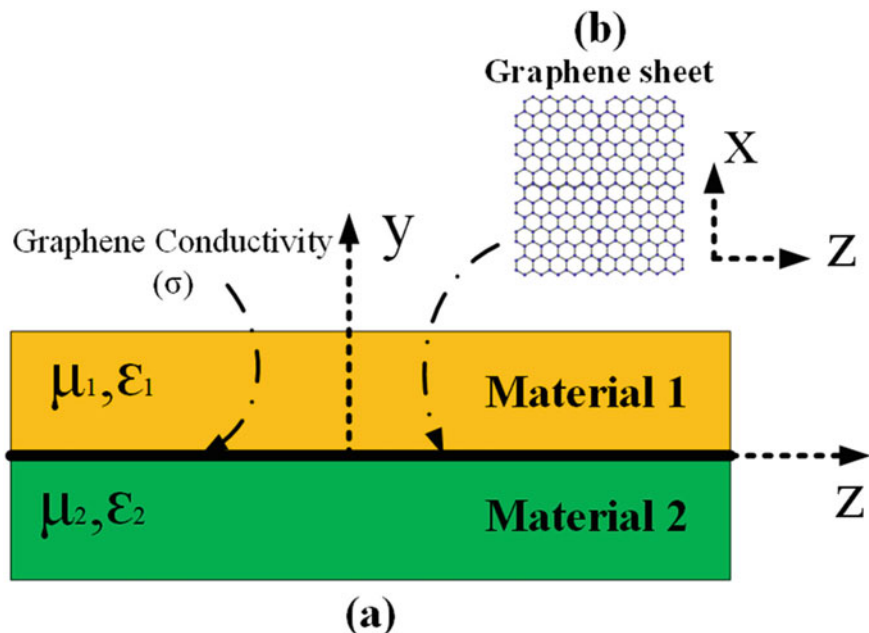
Fig. 1 **a** Graphene as surface conductivity model (σ) between two different materials. **b** Top view of the graphene. Hexagon is denoted as a six atom carbon structure

$$\sigma(\omega, \mu_c, \Gamma, T) = \frac{je^2(\omega - j2\Gamma)}{\pi\hbar^2}\left[\frac{1}{(\omega - j2\Gamma)^2}\int_0^\infty \varepsilon\left(\frac{\partial f_d(\varepsilon)}{\partial\varepsilon} - \frac{\partial f_d(-\varepsilon)}{\partial\varepsilon}\right)d\varepsilon \right.$$
$$\left. - \int_0^\infty \frac{f_d(-\varepsilon) - f_d(\varepsilon)}{(\omega - j2\Gamma)^2 - 4(\varepsilon/\hbar)^2}d\varepsilon\right] \tag{1}$$

Here, ω is defined as the frequency in radian, μ_c is considered as the chemical potential of the graphene sheet. The graphene's chemical potential can be controlled externally. Γ and T are the scattering rate and temperature respectively. Here Γ is assumed to be not dependent on energy. $\hbar$ and e are the reduced Planck constant and charge of electron respectively. The function $f_d(\varepsilon)$ is defined as $f_d(\varepsilon) = \left(e^{(\varepsilon - \mu_c)/k_B T} + 1\right)^{-1}$. Here the local conductivity is considered isotropic by assuming no magnetic field. Equation 1 is categorized in the two conditions as intraband (first part) and interband (second part) conductivity. The carrier density values n_s is used to identify the value of chemical potential μ_c as shown in Eq. 2.

$$n_s = \frac{2}{\pi\hbar^2 v_F^2}\int_0^\infty \varepsilon[f_d(\varepsilon) - f_d(\varepsilon + 2\mu_c)]d\varepsilon \tag{2}$$

where the value of Fermi velocity v_F is considered as approximately 9.5×10^5 m/s. This carrier density can be controlled using external biasing and/or doping voltage. It also needs to consider the for non-doped conditions T = 0K as well as $n_s = \mu_c = 0$.

The intraband conductivity term can be derived as shown in Eq. 3. This equation is first derived by considering the case $\mu_c = 0$ for graphite (by considering the additive factor included for the interlayer connection between two-layer graphene in graphite) intraband conductivity of single-walled carbon nanotube by considering the infinite radius [19]. The simple conductivity, in this case, is considered as real and imaginary part using $\sigma_{intra} = \sigma' + j\sigma''$. Where the values of both part $\sigma'_{intra} \geq 0$ and $\sigma''_{intra} < 0$. The imaginary part of the graphene sheet will help to propagate the surface wave guided by graphene sheet [20].

$$\sigma_{\text{intra}}(\omega, \mu_c, \Gamma, T) = \frac{-je^2 k_B T}{\pi \hbar^2 (\omega - j2\Gamma)} \left(\frac{\mu_c}{k_B T} + 2\ln\left(e^{-\frac{\mu_c}{k_B T}} + 1\right) \right) \qquad (3)$$

The interbrand conductivity for the approximate condition $k_B T \ll |\mu_c|, \hbar\omega$ is presented by Eq. 4. In this equation, the conductivity values are considered from scattering rate $\Gamma = 0$ and $2|\mu_c| > \hbar\omega$, $\sigma_{\text{inter}} = j\sigma''_{\text{inter}}$ and $\sigma''_{\text{inter}} > 0$ conditions. For the conditions of $\Gamma = 0$ and $2|\mu_c| < \hbar\omega$, σ_{inter} are the complex values with $\sigma'_{\text{inter}} = \pi e^2/2h = \sigma_{\text{min}} = 6.085 \times 10^{-5}(S)$ and $\sigma''_{\text{inter}} > 0$ for $\mu_c \neq 0$.

$$\sigma_{\text{inter}}(\omega, \mu_c, \Gamma, T) = \frac{-je^2}{4\pi\hbar} \ln\left(\frac{2|\mu_c| - (\omega - j2\Gamma)\hbar}{2|\mu_c| + (\omega - j2\Gamma)\hbar} \right) \qquad (4)$$

3 Graphene-Based Polarizer

They are generally using the Drude models of conductivity to form conventional polarizers which are based on the quantum well-based semiconductor structure. While the metal's imaginary conductivity part is greater than 0, which is used to design only TM polarizer [21] devices. Some extensive research is available on how graphene conductivity is to be calculated [22]. The results published in Hanon [18] in 2008 include most scholars from the industry. Graphene was equated with a 2D material, The surface conductivity of the graphene was measured using the Kubo formula. Because of its adjustable conductivity, graphene can achieve the properties of a metal or transparent medium under the control of different external applied voltages. The polarization controller can therefore be implemented in TE or TM mode with graphene material that cannot possibly be obtained by previous materials. In this respect, graphene is increasingly attractive as a new material for the development of polarizers.
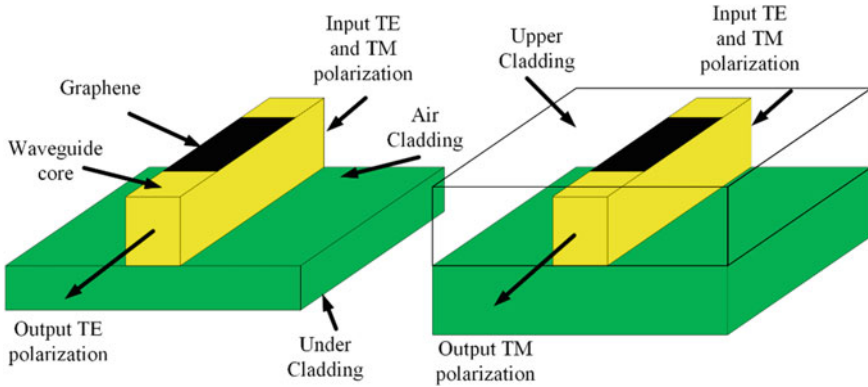
Fig. 2 Schematic structure of polymer-based graphene polarizer device. **a** Growth of the graphene sheet realized. This structure supports the one mode pass (TE mode) polarizer because the air cladding supports a graphene sheet. **b** Modified TM polarizer structure realized by placing the UV curable polymer of CVD grown graphene sheet

There is a huge demand for the creation of compatible photonics integrated circuits with complementary metal-oxide-semiconductor (CMOS) structures. Graphene-based photonics devices are fortunately highly compatible with available conventional CMOS devices. Kim et al. developed a hybrid, optical flat waveguide polarizer. The structure is shown in Fig. 2. In this case, it can be used for selection as a TM or TE pass polarizer to identify whether a top layer cladding is available in the system [23].

The polarizer is based on the graphene-based single-layer sheet. In this structure, both layer (Upper and lower) is formed with per fluorinated polymer acrylate, UV curable, which can adjust graphene's carrier density and conductivity, to allow TM or TE surface waves to be selectively supported. The TE pass polarizer consists of graphene, which consists of a rectangular cross-section corner where the RI is 1.37 and 1.39, as shown in Fig. 2a, respectively. In addition, since in the absence of upper cladding, the waveguide is covered with air. The electrically tunable TM polarizer structure with the graphene monolayer sheet on a guide core as shown in Fig. 2b, The difference between Fig. 2a is only a polymer with a UV curable on top of the layer of the waveguide. The rest of the RI values of the other layer is the same as the TE pass polarizer.

The polymer waveguide with graphene sheet in the polarizer is created first by assembling a lower cladding structure with 20 μm-thick sizes on a silicon slab wafer and then treating it with UV light. The core of the waveguide is transferred to the lower cladding layer, which has a thickness of 5 μm and formed with polymer, which is irradiated with UV light to cure it. The thermochemical vapor deposition (CVD) method has been used to transfer the graphene film on SiO_2/Si substrate. The graphene film for this structure has been grown using thick nickel sputtering with a thickness of 300 nm. The mask is created by photolithography and then modifies

using O_2 plasma to form a linear optical fiber waveguide with graphene tape on the top of the core structure in the polarizer waveguide region.

The graphene polarizer's optical characteristics were tested first by coating it with air. Afterward, the upper layer of the polarizer was formed by spin-coated polymer resin and tested again. To get an infrared image, they did the same as they did with the photometer, except they used the output port of this waveguide structure as a polarized light capturing. The intensity of TE polarized light is observed strongly in the air-clad-based polarizer structure as compared to the TM-polarized light intensity. The key factor is the air-coupling layer. While the UV curable resin layer is been placed on the top of the waveguide in the TM polarizer. After placing this layer, the TM-polarized light is modified to a more intense spot. The TE light has a faint intensity, which may be detectable by polarized light. There is a very small RI difference between the upper and lower layers. Although the slab mode can be seen in TM-polarized light. This structure with UV curable resin work as a TM-polarizing waveguide. Also, the insertion loss is measured in the waveguide to investigate the polarizing effect.

Graphene strips have a notable effect on insertion loss in waveguides with cores. For polarizing TE-treated graphene light, generates the 10.9 dB of the extinction ratio 20.7 dB of the insertion loss. On average, the TE-related modified graphene polarizer had a 50 dB of insertion loss, and the TE insertion loss was found to be 19.8 dB. This results in the majority of the optical power being radiating in a radiative mode. As a result, Kim concluded that the proposed waveguide device takes full advantage of the variation in optical and electrical characteristics concerning external biasing connected to graphene for use in on-chip PICs.

4 Graphene-Based Polarizer Using Optical Fiber

In an optical network, an optical fiber polarizer is one of the most important passive components, as it controls the orientation of the phase and polarization. It is especially popular due to its lightweight, quick rise time, long lifetime, and ease of integration with the optical fiber system (High compatibility). At present, the fiber optic sensing system and fiber gyroscope is the primary device for polarized light generation in the fiber. This system will also play an important role in the optical fiber system. An optical attenuator can be split into an optic polarizer. The difference between two modes of polarization, one stronger and one weaker, is to be increased for creative interference. The longer the mode is used, the less loss it produces, so the shorter the other mode gets. The polarization identity of these two endpoints follow is that one mode of polarization end of the line and the polarization mode flows from it. For the typical fiber, polarizers based on metal-clad fiber, toroidal clad fiber [24], and crystal clad fiber are frequently used [25].

Graphene's outstanding optical and electrical properties mean that its chemical potential can be externally manipulated. The "n-doped" state of graphene can be obtained by adding metals to the atom-doped state of graphene, and the "p-doped"
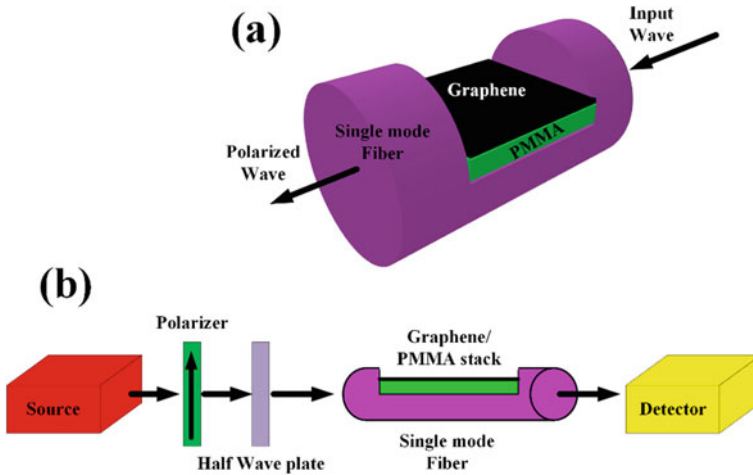
Fig. 3 **a** Schematic of the stacked PMMA/graphene-based fiber-based polarizer structure. **b** Setup for identifying extinction ratio measurement

graphene state can be attained through the introduction of polymer molecules such as F, O, N materials. This can be also attained with other semiconductor elements. Additionally, the surface transfer doping of graphene is containing more stable conditions. While the variationally doping having less unstable conditions than surface transfer doping. The quality of the overall surface coverage of the number of atoms or chemical species or dopant atoms that are mixed into the basal plane is impossible to replicate. We need precise ways to uniformly and precisely dope n-type/p-type graphene for various applications, and then use these methods to control the concentration of dopant. It is possible to effectively suppress the Transverse magnetic and transverse electric modes by controlling the chemical potential of graphene.

Figure 3a shows 3D schematic of the PMMA/Graphene stacked fiber-based polarizer structure and Fig. 3b shows the proposed setup for identifying extinction ratio measurement values. The wheel side-polished method is used to create the polished surface. The fiber polarizer loss is dependent on parameters such as a side-polished facet roughness and the length and surface. The measured fiber polarizer loss was smaller than 1 dB/mm is observed for the polishing depth of 62.5 μm. This loss can be reduced by making a more polished surface. The CVD method is used to grow graphene on copper foil. A spin coater with a very high rotation speed is used to form the 400 nm thick PMMA film.

While this treated copper foil was sitting in ferric nitrate nonahydrate solution for two hours, the rest of the PMMA-graphene surface was flushed with deionized water. The evaporation of any leftover solvent left the fiber materials in contact, which resulted in a single layer of graphene and PMMA. It was coated a second time with a graphene/PMMA sheet and transferred again, yielding a double-sided PMMA stack-based graphene polarizer. Because of a modal evanescent field enhancement associated with the high-index fiber cladding, light can propagate throughout the

core of the fiber. With strong light interaction between the modes, the attenuation between orthogonal polarizations is high, and this results in a lower value of the insertion loss because of the device compactness. When the device is only 2.5 mm in length, a double-layer PMMA/graphene stacked fiber polarizer is composed of a 5 dB insertion loss and a 36 dB extinction ratio. A double-layer of bilayer graphene (on both sides) has outperformed single-layer graphene and single-coated graphene (one side only) in designing and manufacturing polarizers with a ratio of 44 dB for 4 mm device length.

5   Graphene Array-Based Polarizer

Several graphene-based THz polarizers with the composition of other materials have been presented previously [26]. Metasurfaces devices are manipulating EM waves using two-dimensional anisotropic array structures. It is possible to create tunable THz polarizers, either using pure graphene metasurfaces structure or through graphene and metal incorporated metamaterial geometries. These structures can control the polarization direction of the incident light and convert the linear state of polarization to circular polarization states. More interestingly, graphene-based THz polarizers are essential to offer THz attenuator devices for switching devices for THz communications [27]. The wire grids-based THz polarizer with the substrate [28] or free-standing [29] structures offer an approximately 40 dB of high extinction ratio and 1 dB of low insertion loss for lower THz range up to 1 THz [30].

This type of polarizer with metallic wire grid structure shows a high transmission amplitude for TM polarizer wave and low transmission for TE polarized wave [29]. The same effect can be observed for wire grids made up of graphene sheets, for the near-infrared and microwave range [31–33] of the EM wave spectrum. In addition to graphene wire grid structure generates the low transmission for THz waves (TM polarized) with the effect of wave plasmon coupling [34, 35]. This graphene wire grid-based THz polarizers having a limitation of low transmission in both transmission modes. Another limitation in graphene wire grid-based polarizer structure is the low modulation (~10%) (TE mode of polarization), which is created by the Drude absorption [34] effect.

This polarizer is formed such that both metal and graphene elements are interleaved. Metal metasurface in the polarizer structure is fabricated from a graphene grid and metal patch array structure. A graphene sheet is used in the metal grid structure. This offers a higher conductivity than the grid structure formed from individual graphene sheets. The graphene wire hybrid polarizer structure, with graphene wire grid placed onto a metal metasurface, is shown in Fig. 4. The graphene filling factor (GFF) responsible for the conductivity modulation. Smaller values of GFF along the wire make a larger conductivity modulation, which will make larger THz transmission modulation.

The metal metasurface along with the graphene patch wires makes a strong TM-polarized plasmon mode, which causes the separated graphene patch geometry to be

Fig. 4 **a** Three-dimensional view of hybrid wide grid formed with graphene metal-quarts based polarizer structure. **b** Cross-sectional view of the graphene metal quarts based polarizer structure
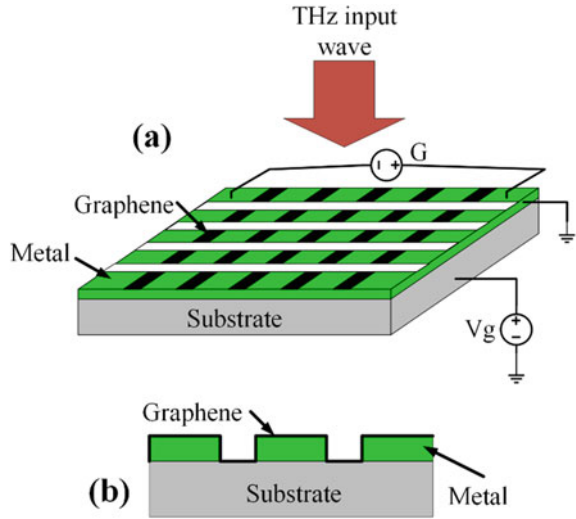
connected with an individual metal strip. The coupling efficiency of wave plasmon interaction is depending on the dimensions of graphene patch up to a certain width, the TM-polarized coupling can be suppressed by decreasing graphene wire length [36]. The metal metasurface provides the TE polarized plasmon into graphene. The polarized plasmon (TE mode) interacts with the THz wave and it will also tunable by different values of graphene conductivity. The THz transmission modulation variation can be realized with these TE polarized plasmons [37]. The metal graphene structure forms the inductive and capacitive circuit which generates the coupling resonance with TE polarized plasmons. In this circuit, charge accumulation is formed by metal and an inductive channel formed by graphene sheet.

The graphene-wide grid-based polarizer is fabricated on ST-cut SSA quartz substrate with 0.35 mm thickness. DLP laser lithography uses to fabricate the metal patterns. In this lithography, the layer of Ti (7 nm) and Au(70 nm) has been formed with electron beam evaporation. The wet transfer procedure [38, 39] is used to transfer the CVD graphene sample on the metal array. The spin coat of the PMMA is taken as support in this process. The copper foil was removed after this using an ammonium persulfate solution with a 2% concentration. Initially, graphene is covered the whole area of the metal surface. The oxygen plasma at 50 W of power has been applied for 2 min to each graphene wire structure. The photoresist material S1813 is used to protect the graphene wire. This photoresist was removed in acetone after etching. The ion gel was prepared by dissolving PVDF-HFP in acetone with the aid of a magnetic stirrer for an hour, before adding the [EMIM][TFSI] into the solution and stirring for 24 h. The gel was prepared with ionized solvent as suggested in [40]. This gel offers large carrier density and good transparency at lower applied gate voltage [41].

6 Graphene Gold Patch-Based Three-Layered THz Polarizer

6.1 Introduction and Design Modeling

The graphene conductivity equation allows to articulation single-layer graphene sheet in various FEM computational platforms as a surface conductivity model. The single-layer graphene-based polarizer structure is numerically investigated as per the structure shown in Fig. 5a. In this structure width and length of the structure (W) are set as 7.6 μm. The size of the patch is set as L set as 4 μm. The height of the
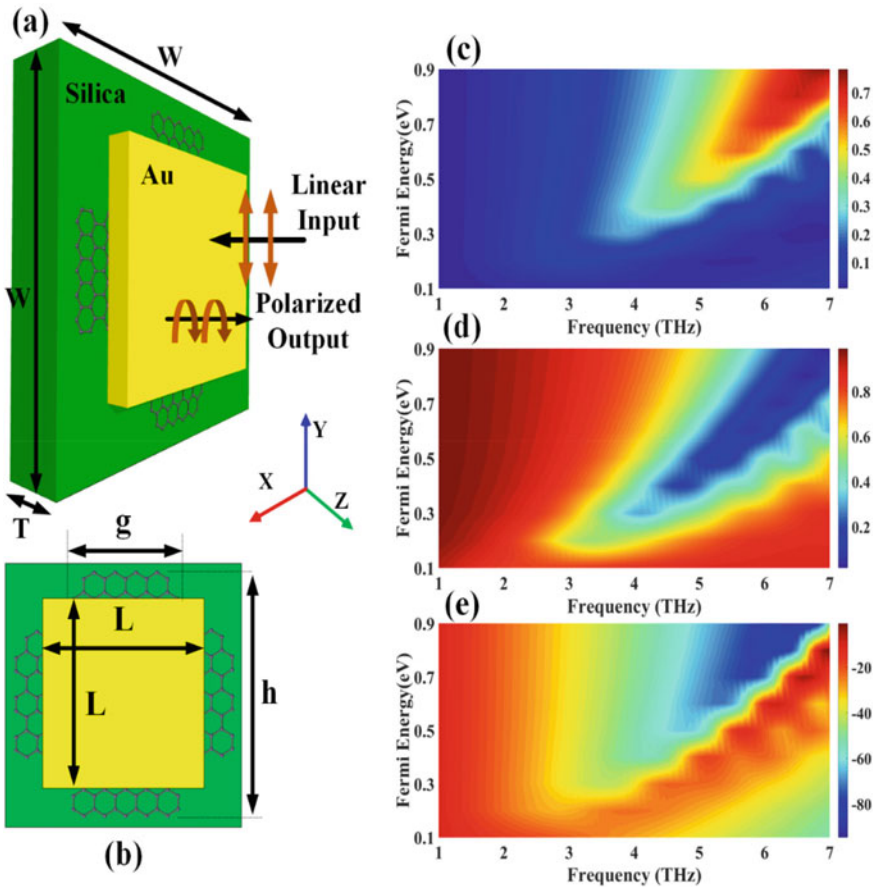

Fig. 5 Graphene-based polarizer structure for THz frequency spectrum. **a** 3D view of the polarizer structure. **b** Top view of the polarizer structure. **c** Reflectance and **d** transmittance amplitude for different fermi energy values of graphene and frequency. **e** Phase variation for the different fermi energy values of graphene and frequency

gold patch is set as 200 nm. The graphene is articulated as a cross-shaped structure with a single-layer structure. The graphene conductivity equation is used as given in Eqs. 1–4. The length and width of the graphene patch are set as ($g \times h$) 3.25 × 6.5 μm. The thickness of the silica is set as 1.5 μm. The wave is excited about the *Z*-axis. *X-Y* boundaries are set as periodic boundary conditions. The reflection and transmitted amplitude variation are calculated by considering the two-port system for the proposed structure. The fermi voltage of the graphene is varying from 0.1 to 0.9 eV for the graphene sheet.

6.2 Results and Discussion

The reflectance and transmittance amplitude variations are shown in Fig. 5c, d. the reflected wave phase change is shown in Fig. 5e. This fundamental structure is used to identify the wave polarization for the THz range and different Fermi energy of the graphene sheet. The reflected wave amplitude and its polarization values help to identify the polarization conversion (linear/circular/elliptical). The comparative table of such layered polarizer devices is shown in Table 1.

Table 1 Comparative study with the proposed polarizer structure and previously studied the structure in terms of various physical parameters

References	Material	Dimensions (W, L, H) in μm^3	Max. reflectance (%)	Type of layer	Wide-angle stability	Min. and max. frequency band
Liu et al. [42]	Metal	(200, 200, 90)	55	Single layer	70	1.6–5
Liu et al. [43]	Metal	(100, 100, 26)	70	Multi layer	40	0.76–1.48
Yu et al. [44]	Graphene dielectric gold	(120, 120, 59)	40	Single layer	–	0.4–1
Fardoost et al. [45]	Graphene	(15, 15, 19)	25	Multi layer	–	1.65–4.35
Deng et al. [46]	Tantalum nitride	(70, 70, 25)	60	Single layer	45	1.17–2.99
Zhu et al. [47]	Graphene dielectric Silica	(16, 16, 25)	22	Single layer	40	0.6–2.6
Shi et al. [48]	Metal	(105, 105, 25)	80	Multi layer	60	0.7–2.5
Gao et al. [49]	Graphene silica	(4, 4, 0.25)	75	Single-layer	–	1–4

7   Graphene Metamaterial-Based Polarizer

Metamaterials, which are not found in nature, are frequently the focus of interest over the last two decades, are experiencing increasing levels of public scrutiny in academic research. a Few kinds of materials can be utilized in the application, including semiconductors [50–52], periodic materials containing multiple metals, which are used in optics and electromagnetics metamaterials, [50–52]. particularly, their property of being able to be expanded to make lightweight or deformable items without being of physical substance is noteworthy until that time static does not prove useful, expansion of metals is unviable, we must restrict development.

The properties of grapheme—an active semiconductor that can also act as a plasmonic device—have recently increased in use as metamaterials have started to be focused on its new dynamic properties [53]. Giant gold nanoparticles have the potential for helping with certain optical devices, especially those with light transmission, this is known as plasmon-induced transparency (PIT) The rule is that if the linearly polarized light enters a semi-transparent glass, the model will shift from clear to opaque. Other than that, dark and bright modes based on the structure of the graphene can be additionally configured with a fermi level, there are bright and dark ones that are based on switching to and lowering or increasing the Fermi level within graphene. PITIs are commonly employed, which may make the PIT phenomenon common. Thus, metamaterials used in this way have also begun to be discovered as a research interest.

The metamaterial structure as a single periodic unit comprising four graphene blocks and strips is shown in Fig. 6a. The linearly polarized light is excited from the
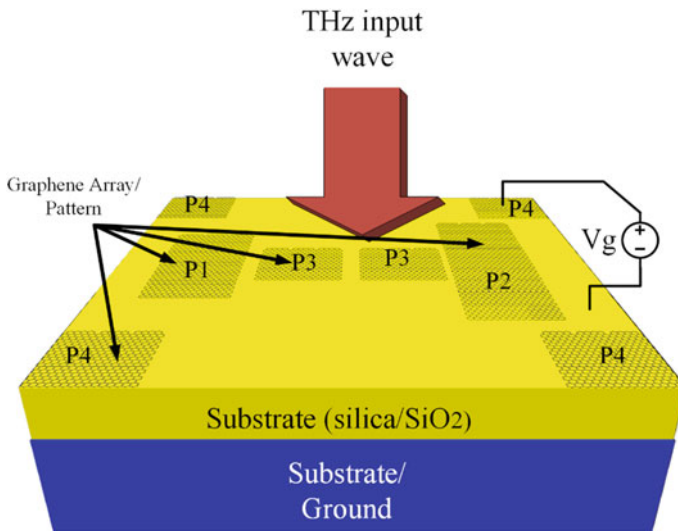

Fig. 6 a Three-dimensional view of the graphene patch array-based polarizer structural unit

top of the structure as shown in Fig. 6. The different graphene metamaterial structure generates different transmission spectrum for the different incident source polarization conditions by exciting different graphene patch on the array. It is possible to design such an array-based graphene polarizer structure using different graphene engraved geometries [54, 55]. Many studies show that the polarization angle of the light will have a great influence on the performance of the metamaterial structure. To check the behavior of the variation in the polarization state in this study the different structures of graphene metamaterial will produce individually. The polarizer structure with only the P1 patch in Fig. 6 will generate the red Lorenz lines for *X* polarization incident conditions. It is possible to generate the bright modes as they are interacting directly with the incident light and graphene in presence of patch P1/P3. This interaction generates the red Lorenz line. However, The polarizer structure with a single P4 patch generates the dark mode as it is not interacting with the direct incident light. Surprisingly, In *Y* polarized light the for all the structures the red Lorenz lines disappear. A graphene structure can produce multiple resonances points. Multiple resonant dips appear at different frequencies for this graphene-based metamaterial structure. In this research study the low-frequency first-order resonance shown; complex phenomenon results for the second or higher order resonating modes. This mode is ignored in the studies. Similarly, in many cases of split ring structure, *I* shaped, *L* shaped, cross-shaped graphene engrave geometry it possible to generates the different polarization effects with different input incident angles.

The applications of the graphene-based polarizer device are shown in Table 2. The graphene-based polarizer is used in many fields such as light manipulation devices, Photodetector, polarization sensors, modulators, radiating antenna, etc. The short working methodology along with the advantages as compared to other non-graphene-based devices are shown in Table 2.

8   Conclusion

Graphene-based THz polarizer has attracted the large attention of the scientific community due to its reconfigurable and ultrathin design. The different graphene-based polarizer structure offers to generate tunability, TE to TM mode conversion, ultrathin design. The graphene-based metamaterial polarizer is used for potential applications such as sensor, photodetector, antenna, modulator, polarizer, etc. In this chapter, we presented various designs and structures of the polarizer with its working principles, fabrication techniques, and advantages. We presented useful mathematical equations to articulate the graphene-based conductivity model which helps to define properties of graphene in FEM calculation. A Three-layer silica-graphene-gold-based structure is numerically investigated using the same graphene conductivity formulation and FEM environment. This chapter will give the idea of forming fundamental graphene-based polarizer and other photonics devices for various THz and electro-optical applications.

Table 2 Application of the graphene-based polarizer devices with working methodology and possible advantages of structure

Type of devices	Working methodology	Advantages
Polarization sensor	• Enhance the absorption values • Use the attenuated total internal reflection	• Fast speed of measurement • Real-time processing • Sensitivity is high • Low sample consumption
Polarization Photodetector	• The different shaped structure used with SiO_2 substrate • Different pattern structure created different surface plasmon • Photodetector tunability achieved using an external biasing voltage of graphene	• Fast and responsive speed • High rate of detection • Works on broad-spectrum and tunable
Polarization modulator	• Absorption is changed concerning the applied voltage by refractive index variation • Light absorption rate controlled by an electrical signal which is ultimately modulation variation	• Small loss • Small volume • Modulation efficiency and extinction ratio is high
Polarizer	• Depends on the leak mode created by the graphene surface • When epsilon reaches zero, one mode loses from TE/TM and one remains available at another side of the structure	• Easy to integrate • Small size • High compatibility with another device • Working on a wideband spectrum
Polarizer based antenna	• Different shape of structure generates different polarized radiation signal • Graphene work as a conductive medium for radiation • Tunable with external biasing	• Thin and small size • Tunable

References

1. R.A. Shelby, Experimental verification of a negative index of refraction. Science (80-.) **292**(5514), 77–79 (2001)
2. R. Singh, E. Plum, W. Zhang, N.I. Zheludev, Highly tunable optical activity in planar achiral terahertz metamaterials. Opt. Express **18**(13), 13425 (2010)
3. T. Maier, H. Brückl, Wavelength-tunable microbolometers with metamaterial absorbers. Opt. Lett. **34**(19), 3012 (2009)
4. A.K. Geim, K.S. Novoselov, The rise of graphene. Nat. Mater. **6**(3), 183–191 (2007)
5. F. Ding, Y. Cui, X. Ge, Y. Jin, S. He, Ultra-broadband microwave metamaterial absorber. Appl. Phys. Lett. **100**(10), 103506 (2012)

6. G.W. Hanson, Dyadic green's functions for an anisotropic, non-local model of biased graphene. IEEE Trans. Antennas Propag. **56**(3), 747–757 (2008)
7. Y. Bai, L. Zhao, D. Ju, Y. Jiang, L. Liu, Wide-angle, polarization-independent and dual-band infrared perfect absorber based on L-shaped metamaterial. Opt. Express **23**(7), 8670 (2015)
8. Y. Guo, T. Zhang, W.Y. Yin, X.H. Wang, Improved hybrid FDTD method for studying tunable graphene frequency-selective surfaces (GFSS) for THz-wave applications. IEEE Trans. Terahertz Sci. Technol. **5**(3), 358–367 (2015)
9. V. Sorathiya, V. Dave, Numerical study of a high negative refractive index based tunable metamaterial structure by graphene split ring resonator for far infrared frequency. Opt. Commun. **456**(June 2019), 124581 (2020)
10. L. Thomas, V. Sorathiya, S.K. Patel, T. Guo, Graphene-based tunable near-infrared absorber. Microw. Opt. Technol. Lett. **61**(5), 1161–1165 (2019)
11. S.K. Patel, V. Sorathiya, T. Guo, C. Argyropoulos, Graphene-based directive optical leaky wave antenna. Microw. Opt. Technol. Lett. **61**(1), 153–157 (2019)
12. V. Sorathiya, S.K. Patel, D. Katrodiya, Tunable graphene-silica hybrid metasurface for far-infrared frequency. Opt. Mater. (Amst) **91**, 155–170 (2019)
13. S.K. Patel, M. Ladumor, V. Sorathiya, T. Guo, Graphene based tunable grating structure. Mater. Res. Express **6**(2), 025602 (2019)
14. J. Parmar, S.K. Patel, M. Ladumor, V. Sorathiya, D. Katrodiya, Graphene-silicon hybrid chirped-superstructure bragg gratings for far infrared frequency. Mater. Res. Express **6**(6) (2019)
15. Y. Niu, J. Wang, Z. Hu, F. Zhang, Tunable plasmon-induced transparency with graphene-based T-shaped array metasurfaces. Opt. Commun. **416**(January), 77–83 (2018)
16. T. Guo, C. Argyropoulos, Broadband polarizers based on graphene metasurfaces. Opt. Lett. **41**(23), 5592 (2016)
17. K. Ziegler, Minimal conductivity of graphene: nonuniversal values from the Kubo formula. Phys. Rev. B **75**(23), 233407 (2007)
18. G.W. Hanson, Dyadic green's functions and guided surface waves for a surface conductivity model of grapheme. J. Appl. Phys. **103**(6) (2008)
19. P.R. Wallace, The band theory of graphite. Phys. Rev. **71**(9), 622–634 (1947)
20. S.K. Patel, V. Sorathiya, S. Lavadiya, Y. Luo, T.K. Nguyen, V. Dhasarathan, Numerical analysis of polarization-insensitive squared spiral-shaped graphene metasurface with negative refractive index. Appl. Phys. B Lasers Opt. **126**(5) (2020)
21. Q. Bao, et al., Broadband graphene polarizer. Nat. Photonics **5**(7), 411–415 (July 2011)
22. A. Pandya, V. Sorathiya, S. Lavadiya, Graphene-based nanophotonic devices, in *Recent Advances in Nanophotonics—Fundamentals and Applications*, IntechOpen (2020)
23. S.K. Patel, V. Sorathiya, S. Lavadiya, L. Thomas, T.K. Nguyen, V. Dhasarathan, Multi-layered Graphene silica-based tunable absorber for infrared wavelength based on circuit theory approach. Plasmonics **15**(6), 1767–1779 (2020)
24. Y. Takuma, H. Kajioka, K. Yamada, High performance polarizers and sensing coils with elliptical jacket type single polarization fibers, in *Optical Fiber Sensors* (1988), p. FEE3
25. S.K. Patel, V. Sorathiya, Z. Sbeah, S. Lavadiya, T.K. Nguyen, V. Dhasarathan, Graphene-based tunable infrared multi band absorber. Opt. Commun. **474**, 126109 (2020)
26. Y.V. Bludov, M.I. Vasilevskiy, N.M.R. Peres, Tunable graphene-based polarizer. J. Appl. Phys. **112**(8) (2012)
27. L.-J. Cheng, L. Liu, Optical modulation of continuous terahertz waves towards cost-effective reconfigurable quasi-optical terahertz components. Opt. Express **21**(23), 28657 (2013)
28. K. Imakita, T. Kamada, M. Fujii, K. Aoki, M. Mizuhata, S. Hayashi, Terahertz wire grid polarizer fabricated by imprinting porous silicon. Opt. Lett. **38**(23), 5067 (2013)
29. F. Yan, C. Yu, H. Park, E.P.J. Parrott, E. Pickwell-MacPherson, Advances in polarizer technology for terahertz frequency applications. J. Infrared, Millimeter, Terahertz Waves **34**(9), 489–499 (2013)

30. A. Ferraro, D.C. Zografopoulos, M. Missori, M. Peccianti, R. Caputo, R. Beccherelli, Flexible terahertz wire grid polarizer with high extinction ratio and low loss. Opt. Lett. **41**(9), 2009 (2016)

31. J.-H. Hu et al., Enhanced absorption of graphene strips with a multilayer subwavelength grating structure. Appl. Phys. Lett. **105**(22), 221113 (2014)

32. J. Wu, Enhancement of absorption in graphene strips with cascaded grating structures. IEEE Photonics Technol. Lett. **28**(12), 1332–1335 (2016)

33. M. Grande et al., Optically transparent microwave polarizer based on quasi-metallic grapheme. Sci. Rep. **5**(1), 17083 (2015)

34. L. Ju et al., Graphene plasmonics for tunable terahertz metamaterials. Nat. Nanotechnol. **6**(10), 630–634 (2011)

35. J.W. You, N.C. Panoiu, Polarization control using passive and active crossed graphene gratings. Opt. Express **26**(2), 1882–1894 (2018)

36. Y. Xia et al., Polarization dependent plasmonic modes in elliptical graphene disk arrays. Opt. Express **27**(2), 1080 (2019)

37. M.M. Jadidi et al., Tunable terahertz hybrid metal–graphene plasmons. Nano Lett. **15**(10), 7099–7104 (2015)

38. G.B. Barin, Y. Song, I. de Fátima Gimenez, A.G.S. Filho, L. S. Barreto, J. Kong, Optimized graphene transfer: influence of polymethylmethacrylate (PMMA) layer concentration and baking time on graphene final performance. Carbon N. Y. **84**, 82–90 (Apr 2015)

39. M.P. Lavin-Lopez, J.L. Valverde, A. Garrido, L. Sanchez-Silva, P. Martinez, A. Romero-Izquierdo, Novel etchings to transfer CVD-grown graphene from copper to arbitrary substrates. Chem. Phys. Lett. **614**, 89–94 (2014)

40. K. Chae et al., Electrical properties of ion gels based on PVDF-HFP applicable as gate stacks for flexible devices. Curr. Appl. Phys. **18**(5), 500–504 (2018)

41. B.J. Kim, H. Jang, S.-K. Lee, B.H. Hong, J.-H. Ahn, J.H. Cho, High-performance flexible graphene field effect transistors with ion gel gate dielectrics. Nano Lett. **10**(9), 3464–3466 (2010)

42. X. Liu, Q. Zhang, X. Cui, Ultra-broadband polarization-independent wide-angle THz absorber based on plasmonic resonances in semiconductor square nut-shaped metamaterials. Plasmonics **12**(4), 1137–1144 (2017)

43. S. Liu, H. Chen, T.J. Cui, A broadband terahertz absorber using multi-layer stacked bars. Appl. Phys. Lett. **106**(15), 1–6 (2015)

44. X. Yu, X. Gao, W. Qiao, L. Wen, W. Yang, Broadband tunable polarization converter realized by graphene-based metamaterial. IEEE Photonics Technol. Lett. **28**(21), 2399–2402 (2016)

45. A. Fardoost, F.G. Vanani, A. Amirhosseini, R. Safian, Design of a multilayer graphene-based ultrawideband terahertz absorber. IEEE Trans. Nanotechnol. **16**(1), 68–74 (2017)

46. G. Deng, J. Yang, Z. Yin, Broadband terahertz metamaterial absorber based on tantalum nitride. Appl. Opt. **56**(9), 2449 (2017)

47. J. Zhu, S. Li, L. Deng, C. Zhang, Y. Yang, H. Zhu, Broadband tunable terahertz polarization converter based on a sinusoidally-slotted graphene metamaterial. Opt. Mater. Express **8**(5), 1164 (2018)

48. C. Shi et al., Compact broadband terahertz perfect absorber based on multi-interference and diffraction effects. IEEE Trans. Terahertz Sci. Technol. **6**(1), 40–44 (2016)

49. E. Gao et al., Dynamically tunable dual plasmon-induced transparency and absorption based on a single-layer patterned graphene metamaterial. Opt. Express **27**(10), 13884 (2019)

50. J. Gu et al., A close-ring pair terahertz metamaterial resonating at normal incidence. Opt. Express **17**(22), 20307 (2009)

51. N.I. Landy, S. Sajuyigbe, J.J. Mock, D.R. Smith, W.J. Padilla, Perfect metamaterial absorber. Phys. Rev. Lett. **100**(20), 207402 (2008)

52. J.B. Pendry, Negative refraction makes a perfect lens. Phys. Rev. Lett. **85**(18), 3966–3969 (2000)

53. Y. Zhang et al., A graphene based tunable terahertz sensor with double Fano resonances. Nanoscale **7**(29), 12682–12688 (2015)

54. X. Zhang et al., Polarization-sensitive triple plasmon-induced transparency with synchronous and asynchronous switching based on monolayer graphene metamaterials. Opt. Express **28**(24), 36771 (2020)
55. V. Dave, V. Sorathiya, T. Guo, S.K. Patel, Graphene based tunable broadband far-infrared absorber. Superlattices Microstruct. **124**, 113–120 (2018)